

**Fig. 2** **a** Components of needle targeting accuracy (TPE) separated into three components: lateral, longitudinal and Euclidean. **b** Intra-interventional validation displays TPE on the left side of the planned trajectory

## Results

20 patients (16 males, 4 females) with 28 liver tumors (20 HCC, 7 CRLM, 1 GIST) of an average diameter of  $17 \pm 9$  mm and average location depth of  $88 \pm 27$  mm, underwent stereotactic CT-guided percutaneous MWA procedures. All patients were anesthetized and respirated using a high-frequency jet ventilation technique in order to reduce the respiratory motion of the liver [4]. Two patients were excluded from the study because of technical issues with the aiming device.

Average co-registration fiducial registration error (FRE) was  $1.0 \pm 0.6$  mm and visual assessment by the interventionalist was enabled using the color-coded blending viewer. Average lateral, longitudinal and Euclidean needle positioning errors (TPE) were  $4.1 \pm 2.6$ ,  $3.7 \pm 3.2$  and  $6.0 \pm 3.3$  mm, respectively (see Fig. 2a).

## Conclusions

Fast and online intra-interventional image fusion and treatment verification module was presented and used to evaluate targeting accuracy of the navigation system on 20 patients. It can conclude that navigated percutaneous microwave ablation is sufficiently with a lateral targeting accuracy ( $4.1 \pm 2.6$  mm). The data suggests, that navigated percutaneous application of microwave ablation is accurate and thus efficacious. Furthermore, navigation support might potentially enlarge the group of patients to whom a minimal invasive approach as an alternative to surgical resection, could be offered. In addition, the available accuracy compares favorably with other navigation approaches [2, 5].

TPE reported by intra-interventional image fusion and treatment verification module might be beneficial for the interventionalist for correcting the depth (longitudinal component) or before making a decision of repositioning the needle (lateral component). Such information might reduce the probability of bleeding or tumour seeding due to avoidance of unnecessary needle re-placements.

In on-going research a multiplanar reconstructions of the CT images will be included into the verification module and their influence on the general performance and usability will be evaluated.

## References

- [1] Flanders VL and Gervais D A. Ablation of liver metastases: current status. *Journal of vascular and interventional radiology*. 2010 August;21(8 Suppl):214–22.
- [2] Wood BJ, Kruecker J, Locklin J, Levy E, Xu S, Solbiati L, et al. Navigation Systems for Ablation. *Journal of vascular and interventional radiology*. 2011 August;21(8):1–19.
- [3] Wallach D, Toporek G, Weber S, Bale R and Widmann G. Comparison of free-hand-navigated and aiming device-navigated targeting of liver lesions. *International Journal of Medical Robotics and Computer Assisted Surgery*. 2013 February; 10(1):35-43.
- [4] Denys A, Lachenal Y, Duran R, Chollet-Rivier M and Bize P. Use of High-Frequency Jet Ventilation for Percutaneous Tumor Ablation. *Cardiovascular and interventional radiology*. 2014 February; 37(1):140-6

## Alternatives for intraoperative imaging in IOERT

V. García-Vázquez<sup>1</sup>, E. Marinetto<sup>1</sup>, P. Guerra<sup>2</sup>, M.F. Valdivieso<sup>3</sup>, F.A. Calvo<sup>4</sup>, E. Alvarado-Vásquez<sup>5</sup>, J.A. Santos-Miranda<sup>5</sup>, C.V. Sole<sup>6</sup>, M. Desco<sup>1</sup>, J. Pascau<sup>1</sup>

<sup>1</sup>Departamento de Bioingeniería e Ingeniería Aeroespacial, Universidad Carlos III de Madrid, Madrid, Spain

<sup>2</sup>Departamento de Ingeniería Electrónica, ETSI Telecomunicación, Universidad Politécnica de Madrid, Madrid, Spain

<sup>3</sup>GMV SA, Tres Cantos, Spain

<sup>4</sup>Departamento de Oncología, Hospital General Universitario Gregorio Marañón, Madrid, Spain

<sup>5</sup>Servicio de Oncología Radioterápica, Hospital General Universitario Gregorio Marañón, Madrid, Spain

<sup>6</sup>Service of Radiation Oncology, Instituto de Radiomedicina, Santiago, Chile

**Keywords** IOERT · Intraoperative imaging · Radiotherapy · CT · Dose distribution

## Purpose

Intraoperative electron radiation therapy (IOERT) is a technique that combines surgery and therapeutic radiation delivered to an unresected tumour or to a post-resection tumour bed, with displacement of uninvolved organs or protection of dose-limiting tissues. The radiation is delivered by a specific applicator docked to the linear accelerator and placed directly over the tumour bed or the residual tumour [1]. Compared to photon radiotherapy, the electron beam dose profile is much steeper, with a characteristic dose gradient (dose becomes lower than 10 % in only a few centimeters). Dose distribution is estimated with an IOERT treatment planning system (TPS) based on radiation attenuation for each tissue type, among other factors. This information is obtained from a patient's preoperative CT image and a scanner-specific calibration that converts CT numbers into physical density. Preoperative CT images cannot represent intra-surgical patient modifications such as retraction and displacement of structures, tumor resection or the use of protections. Several CT imaging devices that could be introduced in the IOERT protocol, either in the surgical room or in the linear accelerator room, may solve these limitations. The purpose of this study is to evaluate the image quality offered by different CT devices when they are used to estimate dose distribution for IOERT treatments.

## Methods

Several CT scanners with potential application in IOERT procedures were studied in this work: a portable C-arm with large field of view (FOV) with 3D imaging capability (O-arm Surgical Imaging, Medtronic, USA), a linear accelerator with on-board kilovoltage cone beam CT (TrueBeam STx, Varian Medical Systems, USA) and a mobile CT (BodyTom Portable CT Scanner, NeuroLogica Corporation, USA). A conventional CT simulator (Aquilion Large Bore CT system, Toshiba, Japan) was used to acquire reference images to obtain gold standard dose estimations.

Two phantoms were acquired with those CT devices: model 062 electron density phantom (CIRS Inc., VA, USA) and model 057 triple modality 3D abdominal phantom (CIRS Inc.). The first phantom was used to estimate for each device the conversion factors from CT numbers into physical density values. Cylindrical regions of interest (ROIs) were drawn centered in every plug of the electron density phantom and outside it. ROI mean values and their corresponding physical densities were the inputs to an in-house implementation of stoichiometric calibration [2]. This process takes into account that the phantom is made of tissue equivalent materials that may duplicate tissue densities but not usually replicate their chemical composition. The output, i.e. the relationship between CT numbers and physical densities, was introduced into the IOERT TPS (radiance, GMV, Spain, [3]) in order to consider patient's tissue inhomogeneity. The abdominal phantom was used to simulate an IOERT scenario (tumour in the paraspinal muscle). In order to protect the right kidney, a

protection disk was placed between the clinical target volume and the right kidney. Abdominal images from all scanners were resampled to 1.5 mm isotropic voxel size and then rigidly registered (normalized mutual information as cost function) in order to place the IOERT applicator exactly in the same position for all scanners. IOERT dose distributions were calculated using the Monte Carlo algorithm (error tolerance 1 %) available in the TPS. The dose distribution estimated using images from every CT device was compared to the gold standard in terms of gamma index with an acceptance criterion of 3 % dose difference and a 3 mm distance-to-agreement. Comparisons were done at regions with dose values either greater than 10 % or greater than 70 %.

### Results

Figure 1 shows the dose distribution for the paraspinal muscle IOERT case. TrueBeam and BodyTom provided more similar results to the CT simulator, while O-arm showed the worst match. Neither the electron density phantom (dimensions  $33 \times 27 \times 5 \text{ cm}^3$ ) nor the abdominal phantom ( $28 \times 20 \times 12.5 \text{ cm}^3$ ) could completely be scanned with O-arm due to its reduced field of view (FOV, diameter 20 cm  $\times$  height 15 cm). The percentage of voxels fulfilling a gamma criteria of 3 %/3 mm was superior to 95 % for TrueBeam (specifically, 98.4 % for regions with dose values greater than 10 and 98.8 % for dose values greater than 70 %) and BodyTom devices (specifically, 98.8 and 100.0 % for high doses). O-arm showed worse results even in high dose regions: 63.1 % of the voxels fulfilled gamma criterion for dose values greater than 10 and 78.3 % of the voxels for high dose values.

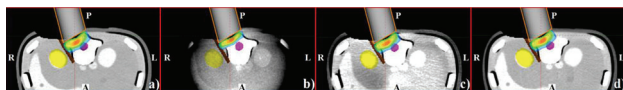


**Fig. 1** Dose distribution in the paraspinal muscle IOERT case: TAC simulator (a), O-arm (b), TrueBeam (c), BodyTom (d)

### Conclusions

Several imaging devices that could potentially be used to obtain intraoperative CT images during IOERT procedures have been assessed in terms of dose distribution values. Two cone beam CT (CBCT) technologies (O-arm and TrueBeam) and a multislice CT (MSCT) were evaluated in this study. Advantages of CBCT technique are lower radiation dose and reduced costs than MSCT but its drawbacks include increased scattered radiation, truncation artefact and not actual HU [4]. Despite of being both CBCT, O-arm showed worse results than TrueBeam. One possible reason for this is the presence of truncation artefacts in the O-arm images that modified their CT numbers. According to our results, a linear accelerator with on-board kilovoltage CBCT or a portable CT could be used to acquire intraoperative imaging in order to update the IOERT dosimetry planning during the surgical procedure.

**Acknowledgments** This work was supported by projects IPT-2012-0401-300000, TEC2010-21619-C04, PI-11/02908, TEC2013-48251-C2, DTS14-00192 and FEDER funds. We would like to acknowledge the support of the Madrid-MIT M+Vision Consortium in facilitating this work. The authors would like to extend their gratitude to GMV, Medtronic, NeuroLogica Corporation, Clínica La Luz, Hospital Universitario Ramón y Cajal, Hospital Universitario La Paz, CIRTS, radiotherapy technicians at Hospital General Universitario Gregorio Marañón, Iván Balsa and Claudia de Molina.

### References

- [1] Calvo FA, Meirino RM and Orecchia R, Intraoperative radiation therapy first part: rationale and techniques.. Crit Rev Oncol Hematol, 59, 106-15, 2006.
- [2] Schneider W, Bortfeld T and Schlegel W, Correlation between CT numbers and tissue parameters needed for Monte Carlo

simulations of clinical dose distributions. Phys Med Biol, 45, 459-478, 2000.

- [3] Pascau J, Santos Miranda JA, Calvo FA et al., An innovative tool for intraoperative electron beam radiotherapy simulation and planning: description and initial evaluation by radiation oncologists. Int J Radiat Oncol Biol Phys, 83, e287-e295, 2012.
- [4] De Vos W, Casselman J and Swennen GRJ, Cone-beam computerized tomography (CBCT) imaging of the oral and maxillofacial region: a systematic review of the literature. Int J Oral Maxillofac Surg, 38, 609-625, 2009.

### Augmented reality system for ultrasound guided radiation therapy

R. Gong<sup>1</sup>, R. Bruder<sup>2</sup>, A. Schweikard<sup>2</sup>, J. Schlosser<sup>3</sup>, D. Hristov<sup>1</sup>

<sup>1</sup>Stanford University, Radiation Oncology, Stanford, United States

<sup>2</sup>Institute for Robotics and Cognitive Systems, Luebeck, Germany

<sup>3</sup>Sonitrac Systems, Menlo Park, United States

**Keywords** Image guided radiotherapy · Robotic ultrasound · Augmented reality · Virtual simulation

### Purpose

The curative potential of external beam radiation therapy is critically dependent on having the ability to accurately aim radiation beams at intended targets while avoiding surrounding healthy tissues. Robotically manipulated ultrasound is a conceptually attractive, cost-effective solution that can be integrated with current medical linear accelerators to address the need for non-ionizing real-time 3D (4D) visualization, localization, and tracking of soft-tissue motion and deformation prior to and continuously throughout treatment beam delivery when accurate targeting is most critical. However, a practical implementation of such solution requires safely incorporating the additional robotic ultrasound hardware in radiotherapy treatment designs without compromising treatment quality in terms of delivered dose distributions. Thus the objective of this work was to develop an augmented reality system to guide the staff towards optimally accommodating robotic ultrasound imaging in the radiotherapy workflow.

### Methods

The MeVisLab environment (Medical Solutions AG and Fraunhofer MEVIS: Bremen, Germany) was used for the development of the augmented reality system. Modules were implemented to support the following data acquisition functionalities: live 3D ultrasound image transfer from an ultrasound scanner via a proprietary Digital Navigation Link (Philips Healthcare); real-time tracking of passive tools with the Polaris (NDI, Waterloo, CA) optical camera, and real-time acquisition of robot axis positions as reported by the robot controller.

High-fidelity virtual models of the robot, the ultrasound transducer with an attached passive tracking tool, and the radiation therapy delivery system (medical linear accelerator) were created as OpenGL Scene Graphs. Both virtual (via widgets) and physical (via live positional updates provided by the optical tracking system and the robot controller) manipulation of the ultrasound transducer and robot models were implemented. The manipulation of the linear accelerator model was realized either interactively (via widgets) or via replay of treatment plans exported as DICOM-RT PLAN objects from a clinical treatment planning system and subsequently imported within the augmented reality environment.

Modules were developed for localizing tracking tools within CT (Computed Tomography) images in order to properly incorporate a CT-based patient model within the system. Furthermore, a GPU algorithm was integrated in a module suggesting candidate ultrasound transducer positions on the patient surface. The CT-patient model and